Slip, Yield, and Bands in Colloidal Crystals under Oscillatory Shear

Itai Cohen,[1,2] Benny Davidovitch,[2] Andrew B. Schofield,[3] Michael P. Brenner,[2] and David A. Weitz[1,2]

[1]*Department of Physics, Harvard University, Cambridge, Massachusetts 02138, USA*

[2]*Division of Engineering and Applied Sciences, Harvard University, Cambridge, Massachusetts 02138, USA*

[3]*School of Physics, University of Edinburgh, Edinburgh, EH9 3JZ, United Kingdom*

(Received 21 November 2005; revised manuscript received 12 August 2006; published 21 November 2006)

We study dense colloidal crystals under oscillatory shear using a confocal microscope. At large strains the crystals yield and the suspensions form shear bands. The pure harmonic response exhibited by the suspension rules out the applicability of nonlinear rheology models typically used to describe shear banding in other types of complex fluids. Instead, we show that a model based on the coexistence of linearly responding phases of the colloidal suspension accounts for the observed flows. These results highlight a new use of oscillatory measurements in distinguishing the contribution of linear and nonlinear local rheology to a globally nonlinear material response.

DOI: 10.1103/PhysRevLett.97.215502 PACS numbers: 61.43.Hv, 47.54.−r, 89.75.Kd

When sheared out of equilibrium, the flow response of many complex fluids is highly non-Newtonian, and nonlinear effects can prevail even for noninertial flow rates. A striking and technologically important phenomenon, common in many complex fluids, is the formation of shear bands where the material separates into regimes characterized by different flows or strain rates [1–5]. Shear bands make rheological measurements notoriously difficult to interpret and can lead to destruction of flow laminarity in various technological applications. Understanding the physical mechanisms for formation and stability of shear-banded flows will reveal key principles underlying the control of complex fluid flows. Shear banding is typically investigated by measuring the material response to steady shear in commercial rheometers. With these methods simultaneous measurements of the full displacement field on the scale of the constitutive particles have been inaccessible [3–5]. Consequently, it has been difficult to distinguish a homogenous sample response, where the entire sample is characterized by the same strain rate, from a heterogenous one, where the sample separates into shear bands with different strain rates. This lack of information also limits the ability to test theoretical descriptions of shear banding that typically assume the material stress response is a nonlinear multivalued function of strain rate [6–8]. As a result, independent confirmations of such models are not available and their predictive capability for more complex time-dependent oscillatory shear, where nonlinear rheology results in anharmonic flow, is limited [9]. Direct flow visualization under time-dependent shear is essential for elucidating the correct material rheology underlying shear banding.

In this Letter we describe measurements using confocal microscopy to image flow profiles of a colloidal crystal under oscillatory shear. At low strains homogenous linear shear gradients are observed throughout the crystal. At sufficiently high strains, bands of low and high strain rates appear, corresponding, respectively, to a crystalline phase and to a smecticlike phase where hexagonally close packed (hcp) colloidal sheets flow over one another [10–15]. The oscillations are purely harmonic with a frequency identical to the one applied. This indicates shear-banding results from coexistence of two linearly responding phases of the suspension. Finally, we present a simple model for shear banding in a linearly responding system that correctly captures the observed behavior.

The suspensions consist of spherical poly-(methyl methacrylate) particles stabilized by a thin layer of poly-12-hydrostearic acid [16]. The particles are impregnated with rhodamine dye and suspended in a mixture of cyclohexyl bromide and decalin, chosen to match the particle density and index of refraction, thus allowing us to image the three-dimensional (3D) structure of the suspension using confocal microscopy [17–19]. The solvent viscosity is $\eta_0 = 0.02$ poise and the particles have a diameter $a = 1.4$ μm and a polydispersity in radius of 5%.

Our shear cell consists of two parallel plates: a movable microscope cover slip and a fixed glass plate 5 mm in diameter. Both plates are flat on the particle scale and parallel to within 1 μm over the entire shear zone. We control the gap separation L, the shear frequency f, and the strain amplitude γ_{app}. A sinusoidally driven piezoelectric actuator translates the cover slip and produces displacements in the x direction of up to 90 μm at $f \leq 100$ Hz. The sample between the shearing plates is in contact with an amorphous suspension with volume fraction $\phi = 0.61 \pm 0.02$ that surrounds the shear zone. The apparatus is mounted on an inverted microscope that allows direct 3D visualization of the sheared suspension.

We prepare a uniform random hcp (rhcp) crystal by preshearing the suspension at $\gamma_{\text{app}} > 1$ and $f = 90$ Hz for at least 1 h. We determine the maximal amplitude of the particle displacement field $|u(z)|$ in the x direction at different heights above the oscillating plate, z. Only samples exhibiting uniform planar structures throughout

the shear zone are considered. Also, we work at gaps large enough to avoid confinement effects [20].

We summarize our data by plotting z as a function of $|u(z)|$ for a wide range of f and γ_{app} (Fig. 1). In each plot, f is fixed and flow profiles at different γ_{app} are compared. For low γ_{app}, we observe a homogenous linear gradient in the displacement amplitude of the crystal, $|u(z)| \sim z$ for all values of f [first two profiles in Figs. 1(a)–1(e)]. At higher strains the crystal yields, and the flow profiles show a surprising f dependence: for $f < 3$ Hz a region close to the upper static plate exhibits a significantly larger strain than that near the lower oscillating plate; this indicates shear banding. The only observed difference in the structures of the two phases is a slightly larger interlayer separation (≈ 0.1 μm) in the flowing hcp phase [21]. The highly strained portion of the sample increases with γ_{app} [Figs. 1(a)–1(c)]. Moreover, the size of the highly strained region increases with f. For $f > 3$ Hz the strain extends across the whole sample [Figs. 1(d) and 1(e)]. While a homogenous crystalline structure is unlikely to exist at such high strains, it is not obvious if the profiles reflect a homogenous response of a noncrystalline phase throughout the gap or thin and thick shear bands corresponding to crystalline and noncrystalline phases, respectively.

Finally, in all the profiles the displacement amplitude of the oscillating plate (solid symbol) is larger than the amplitude of the colloidal hcp sheet adjacent to it (open symbols). Hence there is slip between the plates and the suspension. To characterize the slip, we define the strain induced in the colloidal suspension as $\gamma_{\text{ind}} = [|u(\text{top layer})| - |u(\text{bottom layer})|]/L$ [22] and plot it versus γ_{app} for $f = 60$ Hz [Fig. 1(f)]. The lower slope characterizing the points $\gamma_{\text{ind}} \lesssim 0.1$ indicates a greater fraction of the applied strain is taken up by slip at low γ_{app}.

Shear banding is traditionally studied in samples under steady shear. The standard argument is that shear banding arises from a nonlinear, multivalued rheology [6–8] [Fig. 2(a)]. Since flows where $\frac{d\sigma}{d\dot{\gamma}} < 0$ are unstable, noninertial homogenous flows with $\dot{\gamma}_1 < \dot{\gamma}_{\text{app}} < \dot{\gamma}_2$ must split into bands with distinct values of $\dot{\gamma}$, but identical stress [Fig. 2(a)]. For oscillatory strain the stress must oscillate and change sign. This has two consequences for the nonlinear model: first, since the high shear rate band continuously changes between positive and negative values of $\dot{\gamma}$, the flow must exhibit discontinuous behavior during a full period of oscillation. Second, any nonlinearity in σ would cause the displacement field to respond anharmonically. To test the applicability of such models we measured the temporal flow patterns of different layers in a highly shear-banded flow [Fig. 2(b)]. Remarkably, the colloidal sheets flow in a smooth sinusoidal fashion at the applied f throughout the gap. This striking observation indicates shear banding in our suspension does not reflect a nonlinear local rheology but rather, a linear yet nonuniform response to shear that is characteristic of coexistence between two distinct phases [23].

To model the linear response at low γ we note that at rest the suspension forms a rhcp crystal. This phase remains stable and occupies the entire gap for small strains $\gamma_{\text{ind}} < \gamma_{\text{yield}}$, where γ_{yield} is the yield strain of the crystal. Previous studies established that near equilibrium the crystal stress can be modeled as a sum of viscous and elastic components with effective viscosity η_s and shear modulus G [24,25]. For larger strains $\gamma_{\text{ind}} > \gamma_{\text{yield}}$ a second phase appears, in which the hcp colloidal sheets flow freely over each other signaling a vanishing shear modulus. We model this phase as a Newtonian fluid with effective viscosity η_f. At a given f, the stress in both phases is linearly proportional to the strain [Fig. 2(c)]. The linear rheology of both phases results in harmonic stress response to oscillatory displacements, consistent with the flow pattern in Fig. 2(b).

To account for slip, we also consider flows in the two viscous solvent layers coupling the suspension to the shearing plates. Since $\eta_0 \ll \eta_s$, η_f, the strain in the solvent layers is much larger than in the suspension, leading to the observed slip. For shear flow along $\hat{x}$ with gradient along $\hat{z}$, the off-diagonal components of the stress tensor corresponding to shear stress in the various phases are

$$\sigma_s = G\gamma_s + \eta_s\dot{\gamma}_s \qquad \sigma_f = \eta_f\dot{\gamma}_f \qquad \sigma_{b,t} = \eta_0\dot{\gamma}_{b,t}, \tag{1}$$

where $\gamma = \partial u/\partial z$ is the local strain. Here γ_s, γ_f, γ_b, and γ_t represent time-dependent strains in the solid and fluidlike phases, and bottom and top solvent layers, respectively. Neglecting inertia, γ is uniform in each phase, and $\sigma_s = \sigma_f = \sigma_{b,t}$. For a harmonic response, the coefficients

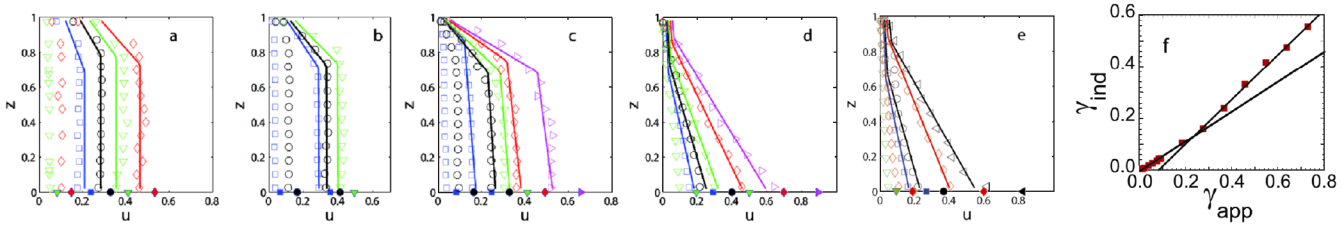

FIG. 1 (color online). Flow profiles for various values of γ_{app} and f. Figures (a)–(e) correspond to f of 0.02, 0.11, 0.5, 15, 60 Hz, respectively. Shown are maximal displacements $|u(z)|$ at several values of z (open symbols). All lengths are normalized by the gap width L. For each profile, the point $(|u(0)|, 0)$ represents the applied amplitude (solid symbols). (f) Plot of γ_{ind} vs γ_{app} for $f = 60$ Hz. The shallow and steep solid lines are linear fits to the $\gamma_{\text{ind}} < 0.1$ and $\gamma_{\text{ind}} > 0.1$ data, respectively.

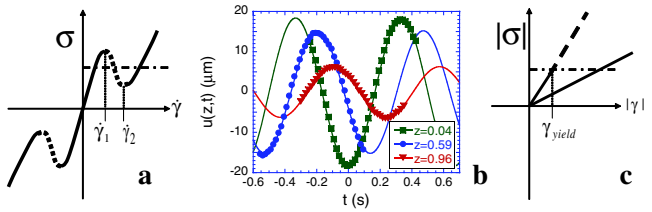

FIG. 2 (color online). (a) Schematic of stress vs strain rate in a nonlinear rheology model for shear banding. The two bands correspond to values of $\dot{\gamma}$ where the horizontal dash-dotted line intersects the solid parts of $\sigma(\dot{\gamma})$. (b) Plots of u vs t for $f = 1.5$ Hz and $\gamma_{\rm ind} \approx 0.6$. The curves correspond to flows in the crystalline ($z = 0.04$) transition ($z = 0.59$) and liquid ($z = 0.96$) regions. The solid lines are fits to the data of the form $u(z, t) = |u(z)|\cos[2\pi f t + \delta(z)]$, where $\delta(z)$ is a phase shift. (c) Schematic of stress amplitude vs strain amplitude in a linear response model for shear banding at a constant applied f. The crystal (top curve) becomes unstable at $|\gamma| = \gamma_{\rm yield}$.

G, η_s, and η_f must be independent of f, γ_s, γ_f. The strains γ_b and γ_t are inversely proportional to the effective thickness of the bottom and top solvent layers d_b and d_t, both of which may depend on ϕ, f, surface chemistry, and packing geometry. The stress field satisfies $\partial\sigma/\partial z = 0$. The general oscillatory displacement field consists of linear profiles in each of the phases:

$$u(z, t)/L = \gamma_{\rm app}{\rm Re}\,[(\alpha + \beta z)e^{i2\pi f t}] \qquad (2)$$

The amplitude and phase lag of the flow field in each phase (solidlike, fluidlike, or solvent layer), are determined by a distinct pair of complex coefficients α, β. The coefficients are found by requiring stress uniformity and continuity of the flow profile. For $\gamma_{\rm ind} < \gamma_{\rm yield}$ the suspension forms a homogenous crystal; there, these requirements yield a unique profile. For shear-banding profiles an additional constraint is needed to solve for the height z^* of the boundary between the fluid and solidlike phases, and to determine a unique solution [26]. We divide the remaining discussion into two parts. First, we address the low $\gamma_{\rm ind}$ regime. Second, we discuss shear banding at $\gamma_{\rm ind} > \gamma_{\rm yield}$.

Case I ($\gamma_{\rm ind} < \gamma_{\rm yield}$ homogeneous).—Since the dynamics are linear, the only nontrivial property of $|u(z)|$ in this regime is the ratio $\gamma_{\rm ind}/\gamma_{\rm app}$. Our model predicts that for a uniform phase $\gamma_{\rm ind}/\gamma_{\rm app}$ must not depend on strain. This corresponds well with our measurements as can be seen from the representative data for $\gamma_{\rm ind} < 0.1$ [Fig. 3(a)]. Similar plateaus for $\gamma_{\rm ind} < 0.1$ are observed at all f. The plateau values of $\gamma_{\rm ind}/\gamma_{\rm app}$ predicted by our model in the limits of high and low f are

$$\gamma_{\rm ind}/\gamma_{\rm app} = \left(\frac{L}{d_s}\right)^2\left[\left(\frac{\eta_0}{G}\right)^2 + \frac{d_s}{L}\frac{\eta_0\eta_s}{G^2}\right](2\pi f)^2, \quad f \to 0 \qquad (3)$$

$$\gamma_{\rm ind}/\gamma_{\rm app} = \frac{\eta_0}{\eta_0 + (d_s/L)\eta_s}, \quad f \to \infty. \qquad (4)$$

Here, we assume symmetry between top and bottom layers $d_s = d_b = d_t$, and that d_s is f independent. For low f, the balance between the f independent elastic stress, which dominates the response of the solidlike phase, and the f dependent viscous stress in the solvent layer, leads to Eq. (3). By contrast, for high f the response in the solidlike phase is also governed by viscous stress; this leads to the f-independent expression in Eq. (4). The crossover between these asymptotic behaviors occurs at $2\pi f_{\rm cross} \sim (d_s/L)G/(\eta_0 + \eta_s d_s/L)$.

We show the f dependence of the plateau values of the ratio $\gamma_{\rm ind}/\gamma_{\rm app}$ in Fig. 3(b). The saturation of $\gamma_{\rm ind}/\gamma_{\rm app}$ predicted by Eq. (4) for high f is confirmed by the data; this trend is independent of the parameter values and therefore strongly supports our linear rheology model, Eq. (1). Moreover, the plateau values of $\gamma_{\rm ind}/\gamma_{\rm app}$ saturate to about $1/2$, from which we obtain: $\eta_s \approx \eta_0(L/d_s)$. The low-$f$ behavior, Eq. (3), is in qualitative agreement with our data. Unfortunately, for systems where $f \ll 0.02$ Hz relaxation mechanisms such as grain boundary motion dominate and our model no longer applies. This makes it hard to verify the low f limit. As a final check, using $f_{\rm cross} \sim 0.1$ Hz and the estimate $G = 0.1$ Pa [25], yields $d_s \sim 0.1$ μm consistent with experiment estimates.

Case II ($\gamma_{\rm ind} > \gamma_{\rm yield}$ shear banding).—Above yielding, excess strain is taken up by a fluidlike phase which either partially or completely fills the gap. The latter case gives rise to shear banding. For $f < 3$ Hz, the region near the oscillating plate remains crystalline with $\gamma \le \gamma_{\rm yield}$ for $0 < z < z^*$ while the region near the static plate ($z^* < z < L$) becomes fluidlike [Figs. 1(a) and 1(b)]. For given f and $\gamma_{\rm app}$ our model predicts a continuous set of shear-banded profiles, parametrized by the variable z^*. This degeneracy can be removed by a selection rule $z^* = z^*(f, \gamma_{\rm app})$, not addressed in our model.

We can compute z^* for each profile by fitting the data to shear-banded solutions solidlike at $z < z^*$ and fluidlike at $z > z^*$. To quantitatively fit the profiles, in addition to z^*, the numerical values of G, η_s, η_f, d_b, and d_t must be determined. Since the solid layer near the plate is exposed to the same conditions as in Case I, we use $d_b = d_s$ which is related to η_s through the relation $\eta_s = \eta_0(L/d_s)$ obtained above. The remaining parameters are determined by data fitting. To insure linearity G, η_s, η_f are taken to be

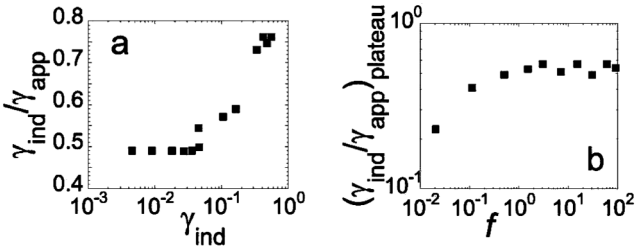

FIG. 3. (a) The ratio $\gamma_{\rm ind}/\gamma_{\rm app}$ vs $\gamma_{\rm ind}$ for $f = 60$ Hz. (b) Plot of the $\gamma_{\rm ind}/\gamma_{\rm app}$ low strain plateau vs f.

independent of f, γ_{app}. While we allow d_t and z^* to depend on f and γ_{app}, only z^* exhibited significant f and γ_{app} dependence. Excellent agreement is achieved between the best-fit profiles [solid lines in Fig. 1(a)–1(e)] and our data. The values of the fitting parameters are $G = 0.2$ Pa, $\eta_s = 0.29$ Pa s (which yields $d_s = 0.04$ μm), $\eta_f = 0.05$ Pa s, and $d_t \approx 0.05$ μm. The viscosities are about 120 and 20 times larger than η_0. The shear modulus agrees well with $G \sim 0.1$ Pa obtained in simulations [25].

Analysis of the high-f flows ($f \geq 3$ Hz, $\gamma_{\mathrm{ind}} > \gamma_{\mathrm{yield}}$) is more challenging since it is difficult to determine whether the profiles reflect a homogenous, fluidlike phase across the sample, or coexistence between solidlike and fluidlike phases. Physically, shear banding is easily observed at low f. Since the stress balance in this regime is dominated by the viscous response in the fluidlike phase and elastic behavior in the solidlike phase, in the limit $f \to 0$, $|\gamma_s|/|\gamma_f| \to 0$ so that the crystalline portion of the suspension is characterized by a very steep region of the flow profile. In contrast, at high f, coexistence requires stress balance between two viscously dominated responses. Thus $|\gamma_s|/|\gamma_f| \to \eta_f/\eta_s$ in this regime, resulting in two tilted linear profiles, with different slopes. Evidence for shear banding can, however, be extracted from the data in Fig. 3(a). As with homogeneous crystal flows, a homogenous fluidlike flow across the gap must give rise to a plateau of $\gamma_{\mathrm{ind}}/\gamma_{\mathrm{app}}$. The data for $\gamma_{\mathrm{ind}} > \gamma_{\mathrm{yield}}$ do not saturate to a constant value; thus, the suspension is unlikely to be composed of a homogenous fluidlike phase. Instead, using the same material parameters obtained from fitting the low f data, we find that solutions of our model that best fit the profiles in the regime $f \geq 3$ Hz and $\gamma_{\mathrm{ind}} > \gamma_{\mathrm{yield}}$ consist of a solidlike phase for $z^* < z < L$ near the static plate and a fluidlike phase at $0 < z < z^*$. These best-fit profiles [solid lines Fig. 1(c)–1(e)] are in good agreement with the data.

In summary, the observed harmonicity of the flows provides clear evidence for the underlying linear rheology in the homogeneous and shear-banding regimes. It is only through the use of oscillatory shear and direct observation of the displacement field that we are able to reveal the linear nature of the rheological response in nonhomogenous flows. Moreover, our ability to directly observe displacement fields on the particles scale should facilitate future studies aimed at determining the mechanical or thermodynamic selection mechanisms of z^*, which is crucial for understanding shear banding in complex fluids. Our results highlight new insights into the rheology underlying inhomogenous flows in complex fluids obtained by combining oscillatory measurements with flow visualization, and suggest similar measurements should be performed on other complex fluids that exhibit shear banding. An interesting question is whether a linear response model, such as the one incorporated here, can be used to describe shear-banding phenomena typically attributed to nonlinear rheology in other systems.

We thank P. Chaikin, H. Stone, L. Mahadevan, A. Sood, D. Blair, and P. Schall for helpful discussions. This work was supported by NSF (No. DMR-0602684, No. DMS-0296056) and the Harvard MRSEC (No. DMR-0213805).

[1] T. C. B. Mcleish and R. C. Ball, J. Polym. Sci. **24**, 1735 (1986).
[2] J. B. Salmon, A. Colin, and D. Roux, Phys. Rev. E **66**, 031505 (2002).
[3] J. K. G. Dhont *et al.*, Faraday Discuss. **123**, 157 (2003).
[4] S. P. Meeker, R. T. Bonnecaze, and M. Cloitre, J. Rheol. (N.Y.) **48**, 1295 (2004).
[5] J. Vermant and M. J. Solomon, J. Phys. Condens. Matter **17**, R187 (2005).
[6] N. A. Spenley, X. F. Yuan, and M. E. Cates, J. Phys. II (France) **6**, 551 (1996).
[7] P. D. Olmsted and C. Y. D. Lu, Phys. Rev. E **56**, R55 (1997).
[8] G. Picard *et al.*, Phys. Rev. E **66**, 051501 (2002).
[9] J. P. Decruppe, S. Lerouge, and J. F. Berret, Phys. Rev. E **63**, 022501 (2001).
[10] N. A. Clark, A. J. Hurd, and B. J. Ackerson, Nature (London) **281**, 57 (1979).
[11] B. J. Ackerson and N. A. Clark, Physica (Amsterdam) **118A**, 221 (1983).
[12] B. J. Ackerson, J. Rheol. (N.Y.) **34**, 553 (1990).
[13] D. Derks *et al.*, J. Phys. Condens. Matter **16**, S3917 (2004).
[14] C. Dux *et al.*, J. Chem. Phys. **104**, 6369 (1996).
[15] M. D. Haw, W. C. K. Poon, and P. N. Pusey, Phys. Rev. E **57**, 6859 (1998).
[16] S. M. Ilett *et al.*, Phys. Rev. E **51**, 1344 (1995).
[17] L. Antl *et al.*, Colloids Surf. **17**, 67 (1986).
[18] E. R. Weeks *et al.*, Science **287**, 627 (2000).
[19] A. D. Dinsmore *et al.*, Appl. Opt. **40**, 4152 (2001).
[20] I. Cohen, T. G. Mason, and D. A. Weitz, Phys. Rev. Lett. **93**, 046001 (2004).
[21] See EPAPS Document No. E-PRLTAO-97-017646 for video of flow fields at different z. For more information on EPAPS, see http://www.aip.org/pubservs/epaps.html.
[22] If slip is localized at one plate the slip length D and γ_{ind} are related by: $D = L\gamma_{\mathrm{ind}}/\gamma_{\mathrm{app}}$.
[23] S. Butler and P. Harrowell, J. Chem. Phys. **118**, 4115 (2003).
[24] A. J. Hurd *et al.*, J. Fluid Mech. **153**, 401 (1985).
[25] D. Frenkel and A. J. C. Ladd, Phys. Rev. Lett. **59**, 1169 (1987).
[26] Assuming solvent layer thicknesses are known, homogenous flows are characterized by 6 coefficients found by solving 6 independent equations: stress uniformity (2), no slip between colloidal phases and solvent layers (2), and no slip between solvent and plates (2). Banded flows are characterized by 8 coefficients and an additional unknown z^*, but only 8 equations are given: stress uniformity (3), no slip between colloidal phases (1), no slip between colloidal phases and solvent layers (2), and no slip between solvent and plates (2).